

Static polarizability of molecular materials: environmental and vibrational contributions

Francesca Terenziani, Anna Painelli

Dipartimento di Chimica GIAF Università di Parma, 43100 Parma, INSTM UdR Parma, Italy

Zoltan G. Soos

Department of Chemistry, Princeton University, Princeton, New Jersey 08544, USA

(Dated: June 14, 2021)

Modeling the dielectric behavior of molecular materials made up of large π -conjugated molecules is an interesting and complex task. Here we address linear polarizabilities, and the related dielectric constant, of molecular crystals and aggregates made up of closed-shell π -conjugated molecules with either a non-polar or largely polar ground-state, and also examine the behavior of mixed-valence (or charge-transfer) organic salts. We recognize important collective phenomena due to supramolecular interactions in materials with large molecular polarizabilities, and underline large vibrational contributions to the polarizability in materials with largely delocalized electrons.

I. INTRODUCTION

A static electric field F applied to an insulating material induces a dipole, $\mu_{ind} = \alpha F + \beta F^2/2 + \gamma F^3/6 + \dots$, whose magnitude depends on the polarizability, α , and hyperpolarizabilities, β , γ, \dots , of the system. Large (hyper-)polarizabilities imply easy redistribution of electronic or nuclear charge by the field. For isolated molecules in the gas phase, the formal theory of static polarizabilities and hyperpolarizabilities is well known, and accurate results can be obtained from quantum chemical calculations on simple molecules.¹ For complex molecular structures the calculation becomes challenging, particularly in large π -conjugated molecules, where important contributions to (hyper-)polarizabilities are expected from molecular vibrations.² For molecules in solution the polarization of the solvent screens the applied fields and the calculation of (hyper-)polarizabilities becomes fairly involved.³

In the solid state, and particularly in crystals, the definition of the dipole moment itself is challenging, and a formal theory for the polarization, P , the dipole moment for unit cell, was developed only in the last decade⁴. The problem is that the polarization of the material apparently depends on the choice of the unit cell.⁵ This problem finds a natural solution in the so-called Berry-phase formulation of P , that relates the macroscopic polarization of the crystal to the ground state (gs) wavefunction rather than to the gs charge-density.^{4,6,7,8} A key concept in the modern theory of polarization is that P is by itself ill-defined and not accessible experimentally: only *variations* of P can in fact be defined as independent of boundary-conditions, and are experimentally accessible.⁸ The Berry-phase formulation of polarizability in insulating materials constitutes an important advance in understanding the electrical properties of crystalline materials, but does not solve the problem of the definition of a dipole moment operator in systems with periodic boundary conditions.^{9,10} A complete and coherent picture for the polarizability (and hyperpolarizability) of crystalline materials is still lacking.

The Berry-phase definition of P is particularly important in covalent insulators, i.e. in crystals such as oxides or silicon, where the charge density is sizeable even between atoms. In organic molecular crystals, by contrast, the overlap between electronic wavefunctions on different molecules is small and there is an unambiguous natural way of partitioning the crystal into an assembly of neutral, localized unit cells (the so-called Clausius-Mossotti limit).^{5,8} In the zero overlap approximation for charge-densities on different molecules, the dipole moment operator for the crystal is simply the sum of the dipole moments of the basic unit cells, and standard approaches to linear and non-linear polarizabilities apply: the formal problem of calculating the crystal polarization and the relevant (hyper)polarizability is trivially solved in this limit. The actual calculation of the electrical responses of molecular crystals is difficult, however, particularly for crystals of highly polarizable molecules. In these materials in fact important collective effects are expected¹¹ and, even if the dipole moment can be calculated as the sum of local dipole moments, the polarizability and the hyperpolarizabilities are not the sum of local contributions.

In this paper we address the calculation of the linear polarizability α in crystalline materials, as related to the experimentally accessible static dielectric constant. Sections 2 and 3 are devoted to the analysis of organic molecular crystals with little or no intermolecular overlap. In these insulators the zero-overlap approximation for charge densities allows to adopt standard expressions for the polarizability tensor, whose Cartesian components $\alpha_{i,j}$ measure the curvature of the gs energy $E_0(F)$ with respect to the field:

$$\alpha_{ij} = - \left(\frac{\partial^2 E_0(F)}{\partial F_i \partial F_j} \right)_0 = 2 \sum_R' \frac{\langle G | \mu_i | R \rangle \langle R | \mu_j | G \rangle}{E_R} \quad (1)$$

The sum-over-state (SOS) expression is the second order correction. It involves the excited states R at energy E_R above the gs at $F = 0$ and the dipole operator μ . The first expression for α above is the finite-field (FF) result, that requires only the gs, albeit at finite fields. We emphasize the long-range nature of electrostatic interactions that lead to significant perturbations to α as due to the environment even in the absence of direct intermolecular overlap. Section 2 reviews a recent approach to the detailed calculation of α in non-polar chromophores with an extended and strongly polarizable π -system. This approach, based on the FF calculation of α for molecules experiencing the electric field generated by the surrounding molecules, relies on quantum chemical models for the isolated molecular fragments and leads to quantitative estimates of the dielectric constant for crystals and films that nicely compare with experimental data.

Section 3 presents an instructive toy model for clusters of polar and polarizable chromophores, based on a two-state picture for each chromophore. Whereas this simple model is hardly quantitative, it correctly grasps the basic physics of supramolecular interactions in these materials. Very schematically, Fig. 1 depicts a polar chromophore in an environment of polar molecules that can be either an ordered crystal or a solution. Electrostatic interactions among dipoles and induced dipoles require a self-consistent treatment that accounts for large local fields due to the dipoles and induced dipoles themselves. Huge collective effects are possible in systems of polar-polarizable molecules, and are indeed expected for certain ranges of parameters. We note that the dipoles in Fig. 1 may represent both electronic and nuclear degrees of freedom or more complicated charge distributions. Quite generally, the zero-overlap approximation for molecular aggregates or crystals leads to such electrostatic problems.

Models with a limited number of states are then particularly instructive for assessing the inevitable approximations in molecular or extended systems. The Born-Oppenheimer (BO) separation of electronic and nuclear degrees of freedom is ubiquitous for molecules and generates potential energy surfaces (PES). In Section 4 we will assess the BO approximation for α in models whose exact eigenstates are accessible, and will present a very simple expression for the vibrational contributions to α that applies in the limit of low vibrational frequencies.

Based on these results, in Section 5 we briefly address the role of vibrational degrees of freedom in charge-transfer (CT) salts with a mixed (donor acceptor, DA) stack motif and variable ionicity. A first description of these materials was given in terms of non-overlapping DA pairs,¹² so that collective effects in α are easily predicted. However, any realistic model for CT salts must account for charge delocalization along the stack. Since the Clausius-Mossotti approximation no longer applies, we resort to Berry-phase polarization and consider P at instabilities. We relate the peak in the dielectric constant observed in some CT salts at a Peierls instability to large charge-fluxes induced along the stack by lattice vibrations.

II. ELECTRONIC POLARIZATION IN ORGANIC MOLECULAR CRYSTALS AND THIN FILMS

The polarization energy of a charge q in a cavity of radius a in medium with dielectric constant κ is $q^2(1 - 1/\kappa)/2a$, or ~ 1 eV for typical $a \sim 5$ Å and $\kappa \sim 3$ in organic molecular crystals.¹³ The major role of polarization has long been appreciated in organic semiconductors.^{14,15} The transport gap E_t for creating an electron-hole pair at infinite separation is reduced from the gas phase value by $P = P_+ + P_-$, the separate stabilization of the cation and anion. The major ($\sim 90\%$) part of P is thought to be electronic,¹⁵ with lattice relaxation or polarons accounting for the rest, and our discussion of P in this Section is restricted to electronic polarization.

We ask how the charge density $\rho(r)$ in the solid differs from the gas-phase density $\rho_G(r)$ of molecules at the same nuclear positions. The crystal induces the difference, $\Delta\rho(r) = \rho(r) - \rho_G(r)$. The lowest-order correction can again be viewed as polarization and rationalized by small overlaps in organic crystals. Organic molecular solids typically have van der Waals contacts and slightly shifted electronic or vibrational excitations, as suggested by the oriented gas model that is the starting point of molecular exciton theory. First-order corrections to energies clearly depend only on $\rho_G(r)$, which can be inferred from gas-phase experiment or theory. Electronic polarization is the first-order correction to $\rho_G(r)$, or to the wavefunction, and is accordingly more difficult to compute.

Small overlap at van der Waals separations suggests starting with zero intermolecular overlap and introducing finite band widths later. In the zero-overlap approximation, charge redistribution $\Delta\rho(r)$ is clearly confined to molecules and intermolecular interactions are purely electrostatic.¹⁶ In this sense, the specific model of polar-polarizable molecules introduced in the next Section represents any aggregate. Conceptually, we have a crystal of quantum mechanical molecules with classical interactions that may be viewed as a non-uniform electric field $F(r)$. Since induced dipoles contribute to $F(r)$, a self-consistent solution is required and made practical by translational symmetry. For example, consider a crystal in a uniform F_{ext} . Since all unit cells have the same total field, we apply constant F and resolve F into local and external fields at the end.¹⁷ The calculation of P_+ or P_- , the polarization energy of an isolated charge, is done in two steps.¹⁶ First, the *extensive* quantity $\Delta\rho_N(r)$ is found for the neutral lattice using translational invariance. Then the *intensive* quantity $\Delta\rho_{\pm}(r, R)$ is found relative to $\Delta\rho_N(r)$ in spheres of radius R about the charge without redistributing charge on molecules whose center is outside the sphere. Convergence to P_{\pm} rigorously goes

as $1/R$ at large R with a slope that depends on the dielectric tensor κ . Representative organic crystals show proper convergence by $R \sim 100$ Å. This corresponds to clusters of thousands of molecules and underscores the long-range nature of polarization. The polarization energy of CT states also requires two steps, again starting with $\Delta\rho_N(r)$. The sphere R now encloses a cation and anion at fixed separation in the crystal lattice. The polarization energy converges faster, as $1/R^3$, since a dipole is enclosed.

The zero-overlap approximation reduces electronic polarization to finding α for molecules in a non-uniform field $F(r)$. This major simplification yields a continuum problem for the functional derivative, $\partial\rho(r)/\partial V(r')$, of the gs charge density at r with respect to the potential at r' . To be practical for crystals or thin films of large molecules, we introduce a discrete approximation for $\partial\rho/\partial V$ by restricting r and r' at molecule a to the atomic positions r_i^a and evaluating $V(r)$ and $F = -\nabla V$ at r_i^a . As done routinely in electrostatic (Madelung) calculations,¹⁸ we represent the gas phase $\rho_G(r)$ by atomic charges $\rho_i^{a(0)}$ at r_i^a . Electronic polarization then yields new atomic charges and induced atomic dipoles that are given by the following linear equations,¹⁶

$$\rho_i^a = \rho_i^{a(0)} - \sum_j \Pi_{ij}^a \phi_j^a \quad (2)$$

$$\mu_i^a = \mu_i^{a(0)} - \tilde{\alpha}_i^a F_i^a \quad (3)$$

Here the sum is over atoms j of molecule a , the electrostatic potential is $\phi_i^a = V(r_i^a)$, and Π is the atom-atom polarizability tensor,

$$\Pi_{ij} = - \left(\frac{\partial \rho_i}{\partial \phi_j} \right)_0 = - \left(\frac{\partial^2 E}{\partial \phi_i \partial \phi_j} \right)_0 \quad (4)$$

that governs how charge redistributes within a molecule. The dipoles μ_i^a contribute to the potential and change according to $F(r_i^a)$. The approximations of zero-overlap and discrete atomic moments lead to eight linear equations per atom, namely the scalars ρ_i^a , ϕ_i^a and the vectors μ_i^a , F_i^a . They are solved iteratively starting with the oriented-gas potential $\phi_i^{a(0)}$ produced by $\rho_i^{a(0)}$. Clusters of thousands of molecules with about 50 atoms each are accessible on workstations.^{16,19}

We comment on general aspects of charge redistribution without going into computational details that are found in refs. 16 and 19. First, semiempirical theory such as INDO/S²⁰ is particularly convenient for Π_{ij} since ϕ_i^a is then simply a site energy; this approximation, typical in solid-state models, is neither the finite-field nor the SOS method of eq. (1), but can be compared to them in exact models. Second, the best gas-phase polarizability α from experiment or theory is retained and partitioned between charge redistribution and a remainder, the $\tilde{\alpha}_i^a$ above. An intuitive partitioning of α in acenes, as done in the submolecular method^{15,21}, leads to self-consistent equations for induced dipoles in external fields. Similarly, the gs dipole μ of polar molecules can be partitioned between charge redistribution and the $\mu_i^{a(0)}$ above. In the spirit of molecular exciton theory, we focus on how $\Delta\rho(r)$ changes in the actual crystal lattice for molecules whose electronic structure is given by hypothesis. Third, polarization energies are bilinear expressions¹⁶ in self-consistent atomic charges and induced dipoles coupled to gas-phase potentials or, vice versa, self-consistent potentials and fields coupled to gas-phase charges or dipoles. Since potentials and fields produced by the best gas-phase charge distribution $\rho_G(r)$ can be evaluated at atomic positions of the crystal lattice, first-order corrections to polarization energies based on discrete $\rho_i^{a(0)}$ can readily be found.²² Such corrections are important in acenes or other systems with electron-hole symmetry and hence $\rho_i^{a(0)} \sim 0$ in the neutral molecule.

The optical dielectric tensor, or indices of refraction, of anthracene crystals has been measured²³ separately and taken together yield the principal values κ_{ii} and uncertainties in Table 1. The principal axes are the crystallographic b axis, by symmetry, and θ is the angle between κ_{11} and a in the ac plane. All calculations are based on the same, INDO/S-based Π_{ij} , but have different molecular α inputs as indicated in the Table, including the experimental polarizability. The triple-zeta basis with field-induced polarization functions from ref. 24 and density functional theory (B3LYP) with a large basis are nearly quantitative, while the oriented-gas value based on $\rho_G(r)$ is clearly not. The dielectric tensor of the crystal includes charge redistribution and induced dipoles whose interactions are treated self-consistently via eqs (2) and (3).

Polarization energies P_+ or P_- are surface rather than bulk measurements.²⁵ As sketched in Fig. 2, photoelectron spectroscopy (UPS) involves P_+ for a cation that is mainly at the surface while inverse photoelectron spectroscopy (IPES) involves P_- . To minimize charging, thin organic films on metallic substrates are used. Recent interest in organic electronic devices is made possible by advances in forming and characterizing crystalline thin films that compensate for the limited mobility of charges. Charge injection then involves polarization at the metal-organic interface. A constant potential surface with image charges is the simplest model of the metal-organic interface. The zero-overlap procedure for electronic polarization, eqs. (2) and (3), is readily extended to surfaces or interfaces.²⁶ We

take N molecular layers based on the crystal, place them in van der Waals contact with the metal, and introduce image charges and dipoles for neutral molecules as well as for ions at specified locations. Instead of spheres of radius R that enclose ions, we use pill-boxes of thickness $2N$ and variable radius. Convergence again requires thousands of molecules and can be monitored with respect to N as well as pill-box radius.

Perylenetetracarboxylic dianhydride (PTCDA) is a good hole conductor and excellent film former, with molecules lying almost flat on the surface.²⁷ It is a prototypical molecule for organic devices. The crystal value for $P = P_+ + P_-$ is 1.82 eV, which is in the expected range.¹⁶ The calculated monolayer value is $P_{mono} = 1.93$ eV.²⁶ The large polarizability of image charges on one side offsets the vacuum on the other side. Accordingly, thick films have reduced $P_{surf} = 1.41$ eV. The 500 meV change between monolayers and thick films agrees quantitatively with UPS, IPES, and tunneling spectra of PTCDA monolayers and films on gold and silver.²⁶ The calculated P at the metal-organic interface, with image charges on one side and crystal on the other, increases to $P_{inter} = 2.21$ eV. The separate values of P_+ or P_- are relevant for matching energy levels to facilitate the injection of holes or electrons. Efficient injection is a major challenge whose pursuit is largely empirical at present, usually without any consideration of polarization.

Pentacene is another widely used molecule, mainly as thin film transistors.²⁸ Its herringbone structure is more common than PTCDA stacks. Pentacene films have the long axis almost normal to the surface, with high conductivity parallel to the surface. The two inequivalent molecules per unit cell are calculated¹⁹ to have slightly (70 meV) different $P = 2.01$ eV in the crystal. P_{mono} differs by only 6 meV from the crystal, while P_{surf} is 0.23 eV less and P_{inter} is 0.13 eV greater.¹⁹ The contrasting structures of pentacene and PTCDA films lead to different electronic polarizabilities that can now be estimated in the well-defined limit of zero overlap rather than just expected on general grounds in anisotropic solids. Similarly, accurate polarization energies are needed for quantitative analyses of transport gaps or of CT states seen in electroabsorption.

In the context of polarizabilities, we close this Section by noting that since the pentacene long axis is almost normal to the metal, the image charges for a cation or anion produce fields along the direction of largest α and redistribute charge to the ends of the molecule. The induced dipoles of adjacent molecules are parallel and close to each other. These repulsive interactions are relieved by redistributing charge toward the molecule's center, as actually found in the self-consistent solution.¹⁹ The field $F(r_i^a)$ at a pentacene ion on a metallic surface vanishes for atoms near the center and ranges from $\pm 10^7$ V/cm for atoms close to and far from the metal. Electronic polarization in organic molecular crystals produces highly non-uniform fields, as found explicitly in pentacene films and studied below in clusters of polar-polarizable molecules.

III. ELECTRONIC POLARIZATION IN CLUSTERS OF POLAR-POLARIZABLE MOLECULES

Important intermolecular effects are expected in materials where several polar and highly polarizable molecules interact. In these materials in fact the local fields generated by the polar molecules strongly affect the charge distribution on the molecules themselves, leading to a non-trivial self-consistent problem. In so-called push-pull chromophores an electron-donor (D) and an electron-acceptor (A) group are linked by a π -conjugated bridge. These intrinsically polar molecules are also highly polarizable due to the presence of delocalized π -electrons. They are also often largely hyper-polarizable, and represent the molecules of choice for second-order NLO applications.²⁹ As originally recognized by Oudar and Chemla,³⁰ the low-energy physics of push-pull chromophores is well described by a two-state picture. The gs resonates between two limiting structures: $|DA\rangle$ and $|D^+A^-\rangle$, that can be taken as the two basis states of a Mulliken model.³¹ These two states are separated by an energy $2z_0$ and are mixed by a matrix element $-\sqrt{2}t$, that, with no loss of generality, will be fixed as the energy unit. The relevant gs is written as $|G\rangle = \sqrt{1-\rho}|DA\rangle + \sqrt{\rho}|D^+A^-\rangle$, where the ionicity ρ only depends on z_0 . ρ is proportional to the gs dipole moment: $\mu_G = \mu_0\rho$ and $\mu_0 = \langle D^+A^- | \hat{\mu} | DA \rangle$. The excited state, $|E\rangle$, is orthogonal to $|G\rangle$ and its dipole moment is $\mu_0(1-\rho)$. The excitation energy is $\omega_{CT} = 1/\sqrt{\rho(1-\rho)}$ and the corresponding transition dipole moment is $\mu_0\sqrt{\rho(1-\rho)}$.

This simple model sets the basis for current understanding of NLO responses of push-pull chromophores and, if extended to account for the coupling to molecular vibrations and solvation effects, it offers a good description of the spectroscopic properties of push-pull chromophores in solution.^{32,33} Here we adopt this model to investigate the role of intermolecular interactions in clusters of polar-polarizable chromophores. We consider a cluster of Mulliken molecules with purely electrostatic interactions. The relevant Hamiltonian is:³⁴

$$\mathcal{H}_{int} = \sum_i (2z_0\hat{\rho}_i - \sqrt{2}t\hat{\sigma}_{x,i}) + \sum_{i,j>i} V_{ij}\hat{\rho}_i\hat{\rho}_j \quad (5)$$

The first term in (5) describes the on-site problem, with $\hat{\rho}_i$ measuring the polarity (i.e. the weight of the zwitterionic state) of the i -th chromophore, and $\sigma_{x/z,i}$ is the x/z -Pauli matrix for the i -site. The second term accounts for electrostatic intermolecular interactions with V_{ij} measuring the interaction between zwitterionic species located on sites i and j .

The Hamiltonian (5) is fairly general. Here we consider 1-dimensional clusters of N equivalent molecules with the three geometries sketched in Fig. 3. We model each zwitterionic molecule as a segment of length l carrying $\pm e$ charges at the D/A ends, so that, for unscreened interactions, V_{ij} is fixed by $v = e^2/l$, the interaction between two charges at unit distance, and r , the interchromophore distance. In any case the specific expression for V_{ij} does not alter the basic physics of the model. The above Hamiltonian is easily written and diagonalized on the 2^N basis obtained from the direct product of the two basis functions, $|DA\rangle$ and $|D^+A^-\rangle$, on each site. By exploiting the translational symmetry we are able to find exactly at least the lowest 30 eigenstates for systems with up to 16 sites.

Fig. 4 shows the evolution of the chromophore polarity with the inverse interchromophore distance, $w = l/r$ for the three lattices sketched in Fig. 3. All results are obtained for $v = 1$; z_0 is fixed to 1 in upper panels, to show the behavior of a chromophore with a neutral (N) ground state in the gas phase ($\rho = 0.15$ at $w = 0$). The bottom panels ($z_0 = -1$) instead describe the behavior of zwitterionic (I) chromophores ($\rho = 0.85$ at $w = 0$). Interchromophore interactions disfavor charge separation in A geometry, and ρ decreases with w in the leftmost panels in Fig. 4, whereas just the opposite occurs for geometry B and C (Fig. 4, middle and right panels). The behavior of an A cluster of I chromophores (Fig. 4(b)) and of B and C clusters of N molecules (Fig. 4(c) and (e), respectively) are particularly interesting. In the first case the isolated chromophore is zwitterionic, but, with increasing w (i.e. by decreasing the interchromophore distance) the molecular polarity decreases down to the cyanine limit ($\rho = 0.5$) reaching the N regime for an interchromophore distance of about 0.7 times the dipole length. Similarly, a neutral isolated chromophore can be driven to the I regime for large enough interactions in either B and C geometries when the interchromophore distance is about one half of the dipole length (B cluster) or about 1.4 times the dipole length (C cluster).

To make contact with experiment, we note that as a first estimate, push-pull chromophores have $\sqrt{2}t \sim 1$ eV. Then $v = e^2/l = 1$ corresponds to typical molecular lengths ($l \sim 15$ Å). For these parameters, an I chromophore in A geometry crosses the I-N interface at $w \sim 1.5$ (panel (b)), i.e. for intermolecular distance of ~ 10 Å, a reasonable situation. Similarly, curves in panels (c) and (e) indicate that the N-I interface is crossed for interchromophore distance of ~ 7 Å and ~ 20 Å for B and C cluster, respectively. Again the inversion of the polarity occurs for reasonable intermolecular distances. As a matter of fact, it has already been predicted³⁵ that the polarity of a polar and polarizable molecule varies and eventually inverts due to environmental interactions. However, most of the approaches presented in the literature on the properties of interacting push-pull chromophores disregard the molecular polarizability and do not allow the molecular polarity to readjust in response to supramolecular interactions. On general ground, push-pull chromophores have large transition dipole moments (~ 5 -10 D) and their permanent dipole moment undergoes a large variation (~ 20 -30 D) upon excitation³³: in samples with a medium-large concentration of chromophores (intermolecular distances ~ 5 -10 Å) interchromophore interactions are a sizable fraction of, or even larger than typical excitation energies (~ 1 -3 eV)³³.

The mf treatment of the previous Section becomes trivial when applied to the above Hamiltonian. In the two-state model in fact a single parameter, ρ_i , fully defines both the molecular gs and local electric fields at the molecular positions. For lattices of equivalent molecules, as in Fig. 3, a single-parameter self-consistent problem results from the mf approach. In particular, within mf the lattice reduces to a collection of non-interacting molecules, each one described by the same two-state Hamiltonian as the isolated molecule, but with a renormalized energy gap between $|DA\rangle$ and $|D^+A^-\rangle$, $z_0 \rightarrow z_0 + m\rho$, where $m = \sum_j V_{ij}/2$. Dashed lines in Fig. 4 show ρ as obtained from the self-consistent solution of the mf problem, and demonstrate that mf offers a quite satisfactory description of the behavior of interacting molecules, at least for not too large interactions.

Within mf it is easy to recognize a qualitative difference between the I to N crossover in repulsive lattices (A) and the N to I crossover in attractive lattices (B and C). With increasing supramolecular interactions in repulsive lattice (A, $m > 0$) the $\rho(z_0)$ curve becomes less negative, whereas it becomes more negative in attractive lattices (B and C, $m < 0$). For large negative m ($m < -2$) a divergent $\frac{\partial \rho}{\partial z_0}$ is expected, marking the occurrence of a discontinuous crossover from the N to the I regime.³⁷ The N-I crossover is located at $z_0 \sim -m/2$, and for large z_0 (> 1) S-shaped $\rho(w)$ curves are calculated within mf. The appearance of a discontinuous crossover in mf treatments of C-lattices was discussed many years ago, and offered a first description of the neutral-ionic phase transition observed in CT crystals with a mixed stack motif.¹² The behavior of the system in the proximity of a discontinuous interface is very interesting, but is beyond the scope of the present work.³⁴

The static susceptibilities of systems described by the Hamiltonian in Eq. (5) are easily obtained from the successive derivatives of the ground-state dipole moment on a static applied field. Since molecular dipole moments, in the proposed toy model, rigorously lie along the molecular axis (say z), a single component of the polarizability tensor (α_{zz}) is relevant. The magnitude of this component is shown in Fig. 5 for parameters corresponding to panels b, c and e in Fig. 4. Continuous lines show exact results and demonstrate that supramolecular interactions non-trivially affect the molecular response.

To clarify the subtle physics governing the responses of molecular clusters, we discuss approximate approaches to the problem. In the simplest and most widely adopted approach the response of a collection of chromophores is calculated as the sum of the responses of a collection of non-interacting molecules with the same geometrical arrangement.³⁶ This

oriented gas approach is however limited to very weak interactions and fails otherwise, since it completely disregards the dependence of ρ on supramolecular interactions. A slightly better approach relies again on the oriented gas approximation, but assigns each chromophore the same ρ as obtained within the mf approximation. The mf-oriented gas estimates of static susceptibilities are reported in Fig. 5 as dotted lines. The strikingly large deviations from exact results are quite unexpected: the gs polarity is fairly accurately calculated within mf, for these parameters. The failure of the mf-oriented-gas approximation appears since the response to an applied field of a molecule in the cluster differs from the response of an isolated molecule to the same field. Much better results can be obtained within mf provided the gs dipole moment of each molecule in the cluster is allowed to readjust to the applied field. A proper FF-mf calculation of the polarizability as the first derivative of the cluster dipole moment on the applied field just represents the (trivial) implementation to the Hamiltonian 5 of the self-consistent treatment described the Section 2. As shown by dashed lines in Fig. 5, this approach nicely compares with exact results, apart from deviations observed in a narrow region around the N-I crossover.

The static linear polarizability is a gs property that can be accurately calculated within mf, provided collective behavior is properly accounted for. Non-linear responses can be obtained within the same approach from the successive derivatives of the gs dipole moment, and collective effects are found to rapidly increase with the order of non-linearity.³⁷ The deviations between dotted and dashed lines in Fig. 5 demonstrate the importance of collective behavior, here due to the non-linear response of polarizable chromophores to the perturbation induced by the surrounding. Material properties are significantly affected by the supramolecular arrangement: linear and non-linear optical properties can be strongly depressed or amplified by tuning intermolecular distances and/or by changing the relative orientation of chromophores, with effects that are more pronounced at intermediate polarities. The design of molecular materials for advanced applications is then a challenging task: the material properties in fact must be optimized at the supramolecular level. The presented model just represents a first step towards *supramolecular* structure-properties relationships.

IV. VIBRATIONAL CONTRIBUTIONS TO α : A TOY-MODEL APPROACH

Both molecular vibrations and lattice phonons are strongly coupled to delocalized electrons and can significantly contribute to susceptibilities. Accounting for vibrational degrees of freedom even within a simple model for molecular materials like that presented in the previous Section is non-trivial. Exact non-adiabatic solution of the relevant problem is already computationally demanding for clusters of just two molecules. In the following we therefore shortly discuss the vibrational contribution to the polarizability of an isolated push-pull molecule. We again describe the chromophore as a Mulliken DA pair (cf Section 3) but also account for Holstein coupling to a vibrational coordinate, Q .² The relevant Hamiltonian is ($\hbar = 1$ and $\sqrt{2}t = 1$):

$$\mathcal{H} = 2z_0\hat{\rho} - \hat{\sigma}_x + \frac{1}{2}(\omega^2 Q^2 + P^2) - \sqrt{2\epsilon_{sp}}\omega Q\hat{\rho} \quad (6)$$

The first two terms in the above equation describe the electronic Hamiltonian (cf previous Section). In the third and fourth terms the vibrational problem is defined in terms of an internal vibrational coordinate, Q , and of its conjugated momentum, P . In particular the two basis states are assigned two harmonic PES with equal frequency (ω) but displaced minima to account for linear e-ph coupling, whose strength is measured by ϵ_{sp} , the relaxation energy of $|D^+A^- \rangle$. Whereas the model can quite easily be extended to account for quadratic coupling (i.e. for different vibrational frequencies in the two basis states), this adds an additional parameter to the model, without affecting the basic physics.³⁸

The exact non-adiabatic eigenstates of the above Hamiltonian are obtained by the numerical diagonalization of the relevant matrix written on the basis of the direct product of the two electronic states $|DA \rangle$ and $|D^+A^- \rangle$, and of the reference vibrational states (i.e. the eigenstates of the harmonic oscillator in the third term of Eq. (6)).³⁹ The basis is truncated by fixing a maximum number of phonon states, M ; the corresponding $2M \times 2M$ matrix can be diagonalized up to fairly large M values, yielding numerically exact non-adiabatic eigenstates. The minimum M required to get convergence depends on the model parameters and on the properties of interest.

The second derivative of the exact non-adiabatic gs energy vs the applied field, gives the exact estimate of the molecular the polarizability. Results obtained for a molecule with $\epsilon_{sp} = 1$ and a few ω values are reported in Fig. 6 (continuous lines). z_0 is tuned in this calculation as to span the whole $0 < \rho < 1$ interval. The dot-dashed line corresponds to the bare electronic susceptibility, α_0 , i.e. to the response of the two-state model with no e-ph coupling. Hence differences between the continuous lines and the dot-dashed line measure the vibrational contribution to the static response.⁴⁰

For actual molecules or complexes, the large number of electronic states makes non-adiabatic calculations very demanding, and the Born-Oppenheimer (BO) approximation is usually invoked. In the BO approximation, the

effective electronic Hamiltonian, $\mathcal{H}_{el} = \mathcal{H} - P^2/2$, is defined by subtracting the nuclear kinetic energy (KE) from the total Hamiltonian. Its diagonalization yields analytical expressions for the ground and excited state potential energy surfaces (PES).⁴⁰ Even if the Hamiltonian in Eq. 6 assigns the two basis states two harmonic PES with equal curvature, the PES for the ground and excited state obtained from the diagonalization of the electronic Hamiltonian have different curvatures and are largely anharmonic.³⁹ The anharmonicity of the potential prevents the analytical solution of the vibrational problem on either the ground or excited state; however, numerically exact vibrational states can be calculated in both manifolds.⁴⁰ In particular, the eigenstates of the harmonic oscillator with frequency ω , centered at the relevant equilibrium position, are a good basis for the vibrational problem on either PES. The corresponding vibrational Hamiltonian is the sum of a KE term, whose matrix elements are trivial in the adopted basis, plus a PE term, whose matrix elements are calculated via numerical integration. Of course the vibrational matrix is diagonalized on a basis truncated to a large enough number of phonon states as to get convergence.

Once BO eigenstates are obtained, the (transition) dipole moments entering the SOS expression can be calculated via numerical integration. The static polarizability calculated within BO approximation is indistinguishable (in the scale of Fig. 6) from the exact one, as long as $\omega \leq 0.2$. Fig. 7 compares non-adiabatic (continuous line) and BO (dashed line) static susceptibility for $\omega = 0.5$, where deviations appear. Of course the BO approximation becomes worse with increasing ω and is totally untenable for $\omega \geq 1$. For push-pull chromophores $\epsilon_{sp} \sim \sqrt{2}t$ and typical vibrational frequencies, $\omega \sim 1000 \text{ cm}^{-1} \ll \sqrt{2}t \sim 1 \text{ eV}$ support the validity of BO.

When applied within a FF approach to susceptibilities, the BO approximation immediately leads to a partitioning of the susceptibility into PE and KE contributions.⁴⁰ Within BO, the lowest eigenstate of the electronic Hamiltonian defines the PE for the motion of nuclei (in the gs manifold, of course). The total gs energy is obtained by adding the nuclear KE to the PE. Then, as long as BO applies, susceptibilities, i.e. the successive derivatives of the gs energy with respect to an applied electric field, can be calculated as sums of PE and KE F -derivatives. The nuclear KE vanishes in the $\omega = 0$ limit, and the (ω -independent) PE polarizability, reported as the dashed line in Fig. 6, represents the zero-frequency limit of the exact polarizability. The electronic polarization of the Holstein DA molecule is analytical² and is reported as the dot-dashed line in Fig. 6. We can now understand the evolution of the vibrational contribution to the polarizability with the vibrational frequency: in the low- ω limit, KE contributions vanish, and the exact curve tends to the limiting PE result. Vibrational contributions are very large in this limit. With increasing ω , the vibrational contributions to the response decrease: in the antiadiabatic limit ($\omega \rightarrow \infty$) the vibrational contributions to the static polarizability vanishes, and the exact curve trivially reproduces the bare electronic response.

The calculation of PE-susceptibilities for the toy-model in Eq. (6) is trivial. More generally it is easily implemented in quantum chemistry calculations and in solid-state models as well, since it only requires the gs energy calculated at the relaxed geometry for different values of an externally applied field. The calculation of KE contribution is more difficult, since the F -dependence of the lowest vibrational state in the anharmonic gs PES is needed. The nuclear KE contributes to susceptibilities in two different ways.⁴⁰ First of all, due to anharmonicity, the molecular geometry in the vibronic gs is different from the equilibrium geometry (corresponding to the minimum of the gs PES). This correction is however very small. The second contribution stems from the F -dependence of the nuclear KE itself: it is this contribution that indeed accounts for the deviations of the exact curves from the (dashed) PE curve (at least in the BO regime, $\omega \leq 0.2$, where non-adiabatic corrections are negligible). KE contributions are of course very small for low ω , but they increase with increasing ω , leading to a suppression of the vibrational amplification of the static polarizability. This is by no means accidental: in the antiadiabatic limit ($\omega \gg \sqrt{2}t$) phonons cannot contribute to the static polarizability and, with increasing ω , KE contributions progressively increase to counterbalance the PE contribution.

KE contributions to the linear polarizability exactly vanish in the harmonic approximation.⁴⁰ In fact, the equilibrium position in any harmonic vibrational state coincides with the bottom of the PES; moreover the nuclear KE is proportional to the harmonic frequency, i.e. to the curvature of the PES. For a parabolic PES, this quantity is obviously independent of Q , and hence of F . Then, in the low ω limit, where KE contributions to susceptibilities are negligible, the exact α (continuous line in Fig. 6) coincides with the corresponding best-harmonic estimate, i.e. with the estimate obtained by modeling the gs PES as the parabola with the exact curvature at the equilibrium. This is not true for hyper-polarizabilities that, in the same $\omega \rightarrow 0$ limit, are strongly amplified by the anharmonicity of the gs PES.⁴⁰ Within the best harmonic approximation,³⁹ α is conveniently partitioned into an electronic and vibrational contribution:

$$\alpha = 2 \left[\frac{\mu_{CT}^2}{\omega_{CT}} + \frac{\mu_{IR}^2}{\Omega} \right] \quad (7)$$

where μ_{IR} is the infrared transition dipole moment and Ω is the frequency of the best harmonic frequency, i.e. the curvature of the gs PES at equilibrium. The vibrational contribution to the linear polarizability is then proportional to the infrared intensity of the coupled mode, at least in the low-frequency regime, where PE contributions dominate the response. We underline that this result only relies on the BO approximation and on the neglect of KE contributions to

the polarizability. It therefore applies in the low- ω limit quite irrespective of the detailed model for the electron-phonon coupling, and also for largely anharmonic PES.

V. DIELECTRIC CONSTANT OF CT SALTS

Charge-transfer (CT) crystals have mixed face-to-face stacks of planar π -electron donors and acceptors as sketched in Fig. 8. Intermolecular overlap is negligible between stacks, but not within stacks where $\pi - \pi$ overlap is indicated by less than van der Waals separation between D and A. The gs consequently has fractional charges ρ at D and $-\rho$ at A sites.⁴¹ Just as an example, in the prototypical material, TTF-CA, at ambient conditions about 0.2 electrons are transferred on average from the donor (tetrathiafulvalene, TTF) to the acceptor (chloranil, CA).⁴² As seen in Fig. 8, a regular stack of centrosymmetric molecules is not polar because there is an inversion center at each site, as in fact occurs in the actual structures. The inversion center is lost on dimerization and the gs becomes ferroelectric if dimerization is in the same sense everywhere. Much as it occurs in attractive lattices in Section 3, Madelung interactions favor charge separation, and a large variation of ρ can be induced by tuning intermolecular distances. At ~ 77 K TTF-CA undergoes a discontinuous phase transition to an I phase with $\rho \sim 0.7$.⁴² Other systems with N-I transitions are known and transitions can be induced by temperature, pressure or by absorption of light. They are a complex and interesting phenomenon:⁴³ both continuous and discontinuous transitions are known and, in all cases, stack dimerization accompanies the charge crossover proving the important role of phonons and of e-ph coupling in these systems.

A sharp peak in the dielectric constant has been observed at the N-I transition of several CT crystals,⁴⁴. It can be understood on general grounds as due to large charge fluxes induced by an applied field near the charge crossover, but microscopic modeling of dielectric peaks is still in progress.⁴⁵ Charges are delocalized along the stack and the zero-overlap approximation does not apply: we need a model for polarization in extended and highly correlated systems. Moreover the lattice (Peierls) phonon that induces dimerization is strongly coupled to electronic degrees of freedom in a manner reminiscent of solitons in polyacetylene.⁴⁶ The Peierls mode in fact induces large charge displacements around the N-I crossover, and vibrational contributions to the polarizability cannot be disregarded.

The electronic structure of mixed stack CT salts can be described in terms of a Hubbard model with only on-site electron-electron repulsion (U) explicitly accounted for, and modified to account for the alternation of on-site energies, Δ .⁴⁷ This model accounts only implicitly for Madelung interactions and hence describes only continuous N-I transitions. We also account for the coupling to the Peierls phonon, described by δ , as follows:⁴⁹

$$H = - \sum_{i,\sigma} [1 + (-1)^i \delta] (c_{i,\sigma}^\dagger c_{i+1,\sigma} + H.c.) + U \sum_i \hat{n}_{i,\sigma} \hat{n}_{i,\sigma'} + \Delta \sum_{i,\sigma} (-1)^i c_{i,\sigma}^\dagger c_{i,\sigma} + \frac{N}{2\epsilon_d} \delta^2 \quad (8)$$

where $c_{i,\sigma}^\dagger$ creates an electron with spin σ on the i -th site and $\hat{n}_{i,\sigma} = c_{i,\sigma}^\dagger c_{i,\sigma}$. The last term in the above Hamiltonian measures the bare elastic energy associated with the dimerization mode, with $1/\epsilon_d$ measuring the lattice stiffness. The rigid lattice has $\epsilon_d = 0$.

For $\Delta \gg U$ the Hamiltonian (9) describes an almost N lattice ($\rho \rightarrow 0$) of donors and acceptors, whereas for $U \gg \Delta$ an almost I lattice of spin 1/2 radical ions is obtained ($\rho \rightarrow 1$).⁴⁷ The two phases are qualitatively different, with the I lattice being unconditionally unstable to dimerization (spin-Peierls transitions,⁴⁸). The N-I crossover can consequently be identified precisely even for continuous ρ in the rigid regular stack.⁴⁷ Conditional instability in the N regime implies that soft lattices dimerize on that side before reaching the N-I crossover.⁴⁹ The Peierls phonon induces large charge fluxes along the chain with effects that increase the nearer the dimerization transition is to the N-I crossover of the rigid lattice.

By exploiting the recent definition of polarization in extended systems⁴, we were able to demonstrate huge peaks in the IR intensity of the Peierls mode at the structural instability.⁴⁹ But, as shown in the previous Section for Holstein modes, the IR intensity of vibrational modes is quite naturally related to the system's polarizability. We draw two inferences: first, peaks in the static dielectric constant near the neutral-ionic phase transition have a large contribution from vibrational degrees of freedom; second such peaks in soft lattices are associated with the Peierls transition and occur at $\rho < 1/2$. We anticipate that the Hamiltonian (9) or a closely related model will describe dielectric peaks.

Since lattice phonons have low frequencies ($< 100 \text{ cm}^{-1} \ll t \sim 0.2 \text{ eV}$), the BO approximation applies and the KE contribution to α can be safely neglected. The calculation of the vibrational contribution to α in Eq. (7) is simple, given the IR intensity of the relevant model. But the electronic contribution to α is difficult for correlated electrons and will be presented separately.⁴⁵

As a first estimate of the relative importance of the electronic and vibrational contributions, we consider the $U = 0$ limit of uncorrelated electrons in (9), whose electronic α has long been known.⁵⁰ $U = 0$ results are reported in Fig.

9 for $\epsilon_d = 0.28$, which is a fairly stiff lattice that approximates TTF-CA. The static dielectric constant is related to polarizability by the standard expression: $\kappa = 1 + (\alpha_{el} + \alpha_{vib})/\kappa_0$, where κ_0 is the permittivity of vacuum and α is the polarizability per unit cell. We took TTF-CA lattice parameters as typical for CT crystals. Moreover, for the sake of simplicity, we neglected the softening of the Peierls mode at the transition, by simply substituting the Ω entering the expression for the vibrational polarizability in Eq. (7) with the reference frequency $(1/\epsilon_d)$. Thus the estimated vibrational contribution to κ is a lower limit.

The magnitude of electronic and vibrational contributions to κ is similar for noninteracting electrons. Yet the peak at the Peierls instability in Fig. 9 clearly has a vibrational origin. The physical basis of this behavior lies in the large charge fluctuations generated by Peierls phonons in the vicinity of a charge instability, and underlines once more the importance of properly accounting for e-ph coupling in systems with delocalized electrons. All material properties, including *electronic* responses are in fact non-trivially affected by coupling to nuclear motions. The electronic contribution, by contrast, is dominated in $U = 0$ systems by the gap between the valence and conduction band of (9). This gap is almost constant⁵¹ at equilibrium in the dimerized lattice, with increasing δ offsetting decreasing Δ in Fig. 9 to give an almost constant κ_{el} .

Electronic correlations decrease α_{el} and stabilize the I phase of radical ions. CT salts are correlated systems with large U in (9). Although their dielectric constants are not expected to resemble $U = 0$ results, the Peierls instability on the N side nevertheless ensures a strong vibrational peak where α_{el} is monotonic. And increasing dimerization still produces a gap in the electronic excitations $E_R > 0$ in (1) that reduces α_{el} at the N-I interface. Some key $U = 0$ features are expected to be retained in CT salts.

VI. CONCLUSIONS

Modeling the dielectric behavior of molecular materials made up of strongly polarizable molecules is challenging in several respects. Even in traditional molecular crystals where the overlap of charge densities on different molecules can be safely neglected, the self-consistent interplay between local electric field and molecular polarizabilities (and hyperpolarizabilities) is responsible for the appearance of large collective effects: the response of the material is quantitatively, and possibly even qualitatively different from the behavior of a collection of non-interacting molecules. In Section 2 a recent approach to the calculation of the dielectric constant of molecular crystals and films made up of large π -conjugated and non-polar molecules is summarized. The approach is based on the mf approximation, so that the problem for N interacting molecules reduces to the self-consistent problem of a single molecule experiencing the local electric field generated by the surrounding molecules. The new approach to electronic polarization also yield the polarization energies of cations, anions, and CT states, and it is applicable to crystalline thin films.

Even larger effects are expected in materials made up of polar and polarizable molecules, such as push-pull chromophores. A simple toy-model for these materials is based on a two-state description of each molecular unit. Few-state models, while less accurate than quantum-chemical descriptions, yield a more transparent description of the basic physics of the system, and, being amenable to exact solution, offer valuable information on the validity of approximations necessarily introduced when handling more complex Hamiltonians. Results in Section 3 confirm the reliability of mf approximation as introduced in Section 2 for linear (and non-linear) electric susceptibilities of molecular materials with non-overlapping charge distributions. Exact results for the toy-model also confirm the importance of collective effects in aggregates of polar-polarizable chromophores, in which supramolecular interactions can tune molecular polarity over a wide range.

Few state models are also useful to address vibrational contributions to polarizabilities, and particularly to assess the reliability of standard approximation schemes including the BO separation of nuclear and electronic degrees of freedom and the harmonic approximation. A reduced on-site basis, and hence models with few local states, are also a useful starting point to face the challenging problem of polarizability in covalent insulators, such as CT salts. Electronic (charge) instabilities and lattice instabilities coexist in these materials and compete and/or cooperate in complex and interesting ways. The peak in the dielectric constant of several CT salts is due to the Peierls mode and provides another example of intimate coupling between electronic and vibrational degrees of freedom.

Acknowledgments

The work on vibrational contributions to polarizabilities and hyperpolarizabilities in molecular materials and in CT crystals was performed in collaboration with Luca del Freato. The self-consistent treatment of molecular crystals was done in collaboration with Eugene Tsiper. We also thank colleagues for many discussions: Alberto Girlando in Parma, and Jessica Sin, Robert Pascal, Jr., and Antoine Kahn in Princeton. Work in Parma was supported by

Ministero Istruzione Universita' e Ricerca (COFIN-2001), and by INSTM (PRISMA-2002). Work at Princeton was partially supported by the National Science Foundation through the MRSEC program under DMR-9400632.

-
- ¹ D. M. Bishop, Rev. Mod. Phys. **62**, 343 (1990), and references therein.
 - ² A. Painelli, Chem. Phys. Lett. **285**, 352 (1998); and references therein.
 - ³ P. Norman, P. Macak, Y. Luo, and H. Agren, J. Chem. Phys. **110**, 7960 (1999).
 - ⁴ R. Resta Phys. Rev. Lett., **80**, 1800 (1998).
 - ⁵ I. Souza, T. Wilkens, R. M. Martin, Phys. Rev. B **62**, 1666 (2000).
 - ⁶ R. D. King-Smith, and D. Vanderbilt, Phys. Rev. B **47**, 1651 (1993).
 - ⁷ G. Ortiz, R. M. Martin, Phys. Rev. B **49**, 14202 (1994).
 - ⁸ R. Resta Rev. Mod. Phys. **66**, 899 (1994).
 - ⁹ I. Souza, J. Iniguez, D. Vanderbilt, Phys. Rev. Lett. **89**, 117602 (2002).
 - ¹⁰ G.-M. Rignanese, F. Detraux, X. Gonze, A. Bongiorno, A. Pasquarello, Phys. Rev. Lett. **89**, 117601 (2002).
 - ¹¹ J. I. Krugler, C. G. Montgomery, H. M. McConnell, J. Chem. Phys. **41**, 2421 (1964).
 - ¹² Z. G. Soos, H. J. Keller, W. Moroni and D. Nothe, Ann. N. Y. Acad. Sci., **313**, 442 (1978).
 - ¹³ F. Gutmann and L. E. Lyons, *Organic Semiconductors*, Wiley, New York (1967), Ch. 6. 2.
 - ¹⁴ M. Pope and C. E. Swenberg, *Electronic Processes in Organic Crystals*, Clarendon, Oxford, (1982).
 - ¹⁵ E. A. Silinsh and V. Čápek, *Organic Molecular Crystals*, AIP Press, New York, (1994).
 - ¹⁶ E. V. Tsiper and Z. G. Soos, Phys. Rev. B **64**, 195124 (2001).
 - ¹⁷ Z. G. Soos, E. V. Tsiper and R. A. Pascal, Jr., Chem. Phys. Lett. **342**, 652 (2001).
 - ¹⁸ R. M. Metzger, *Crystal Cohesion and Conformational Energies*, Topics in Current Physics, Vol. 26, Springer-Verlag, Berlin, (1981).
 - ¹⁹ E. V. Tsiper and Z. G. Soos, Phys. Rev. B (in press).
 - ²⁰ M. C. Zerner, G. H. Loew, R. F. Kirchner and U. T. Mueller-Westerhoff, J. Amer. Chem. Soc. **102**, 589 (1980).
 - ²¹ J. W. Rohleder and R. W. Munn, *Magnetism and Optics of Molecular Crystals*, Wiley, New York (1992).
 - ²² J. M. Sin, E. V. Tsiper and Z. G. Soos, Europhys. Lett., **60**, 743 (2002).
 - ²³ N. Karl, H. Rohrbacher and D. Siebert, Phys. Stat. Solidi A **4**, 105 (1971); R. W. Munn, J. R. Nicholson, H. P. Schwob and D. F. Williams, J. Chem. Phys. **58**, 3828 (1973); I. Nakada, J. Phys. Soc. Jpn. **17**, 113 (1962); A. N. Winchell, *The Optical Properties of Organic Compounds*, second ed., Academic Press, New York (1954).
 - ²⁴ H. Reis, M. G. Papadopoulos, P. Calaminici, K. Jug and A. M. Köster, Chem. Phys. **261**, 359 (2000).
 - ²⁵ W. R. Salaneck, K. Seki, A. Kahn, J.-J. Pireaux, Eds. *Conjugated Polymer and Molecular Interfaces*, Marcel Dekker, New York (2001. 14).
 - ²⁶ E. V. Tsiper, Z. G. Soos, W. Gao, A. Kahn, Chem. Phys. Lett., **360**, 47 (2002).
 - ²⁷ S. R. Forrest, Chem. Rev. **97**, 1783 (1997).
 - ²⁸ G. Horowitz, Adv. Mater. **10**, 365 (1998); H. E. Katz, J. Mater. Chem. **7**, 369 (1997).
 - ²⁹ S. R. Marder, B. Kippelen, A. K.-Y. Jen, and N. Peyghambarian, Nature **388**, 845 (1997).
 - ³⁰ J. L. Oudar and D. S. Chemla, J. Chem. Phys. **66**, 2664 (1997).
 - ³¹ R. S. Mulliken, J. Am. Chem. Soc. **74**, 811 (1952).
 - ³² A. Painelli and F. Terenziani, J. Phys. Chem. A **104**, 11041 (2000); F. Terenziani, A. Painelli, and D. Comoretto, *ibid.* **104**, 11049 (2000).
 - ³³ B. Boldrini, E. Cavalli, A. Painelli, and F. Terenziani, J. Phys. Chem. A **106**, 6286 (2002).
 - ³⁴ A. Painelli, F. Terenziani, J. Amer. Chem. Soc., **125**, 5624 (2003).
 - ³⁵ C. Reichardt, Chem. Rev. **94**, 2319 (1994).
 - ³⁶ Y. V. Pereverzev, O. V. Prezhdo, L. R. Dalton, Chem. Phys. Lett. **340**, 328 (2001).
 - ³⁷ A. Painelli, and F. Terenziani, Synth. Metals, in press.
 - ³⁸ A. Painelli, A. Girlando, J. Chem. Phys. **84**, 5665 (1986).
 - ³⁹ L. Del Freo and A. Painelli, Chem. Phys. Lett. **338**, 208 (2001).
 - ⁴⁰ L. Del Freo, F. Terenziani, and A. Painelli, J. Chem. Phys. **116**, 755 (2002).
 - ⁴¹ Z. G. Soos and D. J. Klein, in *Molecular Associations*, edited by R. Foster (Academic, London, 1975), Vol. 1, Chap. 1.
 - ⁴² J. B. Torrance, J. E. Vazquez, J. J. Mayerle, and V. Y. Lee, Phys. Rev. Lett. **46**, 253 (1981); J. B. Torrance, A. Girlando, J. J. Mayerle, J. I. Crowley, V. Y. Lee, P. Batail, and S. J. LaPlaca **47**, 1747 (1981).
 - ⁴³ S. Horiuchi, Y. Okimoto, R. Kumai, and Y. Tokura Science **299**, 229-232 (2003).
 - ⁴⁴ S. Horiuchi, Y. Okimoto, R. Kumai, and Y. Tokura, J. Amer. Chem. Soc., **120**, 7379 (1998).
 - ⁴⁵ Z. G. Soos, S. A. Bewick, A. Painelli, A. Peri, in preparation.
 - ⁴⁶ A. J. Heeger, S. Kivelson, R. S. Schrieffer, and W.-P. Su, Rev. Mod. Phys. **60**, 781 (1988).
 - ⁴⁷ Y. Anusooya-Pati, Z. G. Soos, A. Painelli, Phys. Rev. B **63**, 205118 (2001).
 - ⁴⁸ J. W. Bray, L. V. Interrante, I. S. Jacobs, and J. C. Bonner, in *Extended linear chain compounds*, J. S. Miller Ed., Plenum, New York (1983), Vol. 3, p. 353.
 - ⁴⁹ L. Del Freo, A. Painelli, and Z. G. Soos, Phys. Rev. Lett. **89**, 27402 (2002).
 - ⁵⁰ C. Cojan, G. P. Agrawal, and C. Flytzannis, Phys. Rev. B **15**, 909 (1977).

⁵¹ M.J.Rice, and E.J.Mele, Phys.Rev.Lett. **49**, 1455 (1982).

Molecular Inputs	κ_{11}	κ_{bb}	κ_{33}	θ
Expt. (Ref. ²³)	2.49(10)	3.07(10)	4.04(20)	28(2) $^\circ$
TZVP-FIP (Ref. ²⁴)	2.35	3.09	4.31	31.8 $^\circ$
B3LYP/6-311++G(d,p)	2.23	2.91	4.03	31.6 $^\circ$
Expt. gas-phase α	2.69	3.14	3.39	31.6 $^\circ$
Oriented gas	1.36	2.39	3.90	

TABLE I: Principal components of the dielectric tensor and indices of refraction, $\kappa = n^2$, of crystalline anthracene. The calculated κ are based on the indicated molecular α . The unique axis is κ_{bb} ; κ_{11} , κ_{33} are in the ac plane and θ is the angle between κ_{11} and a .

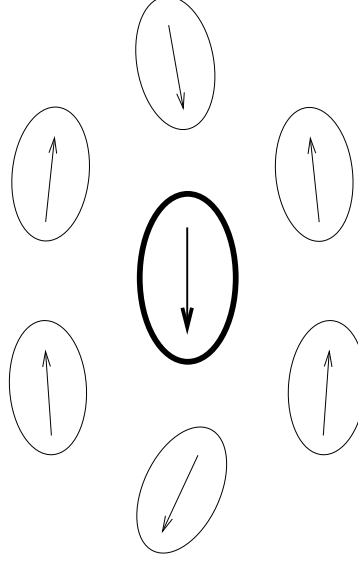


FIG. 1: Schematic view of dipolar molecule interacting with the surroundings, not drawn to minimize energy. The arrows represent both dipoles and induced dipoles.

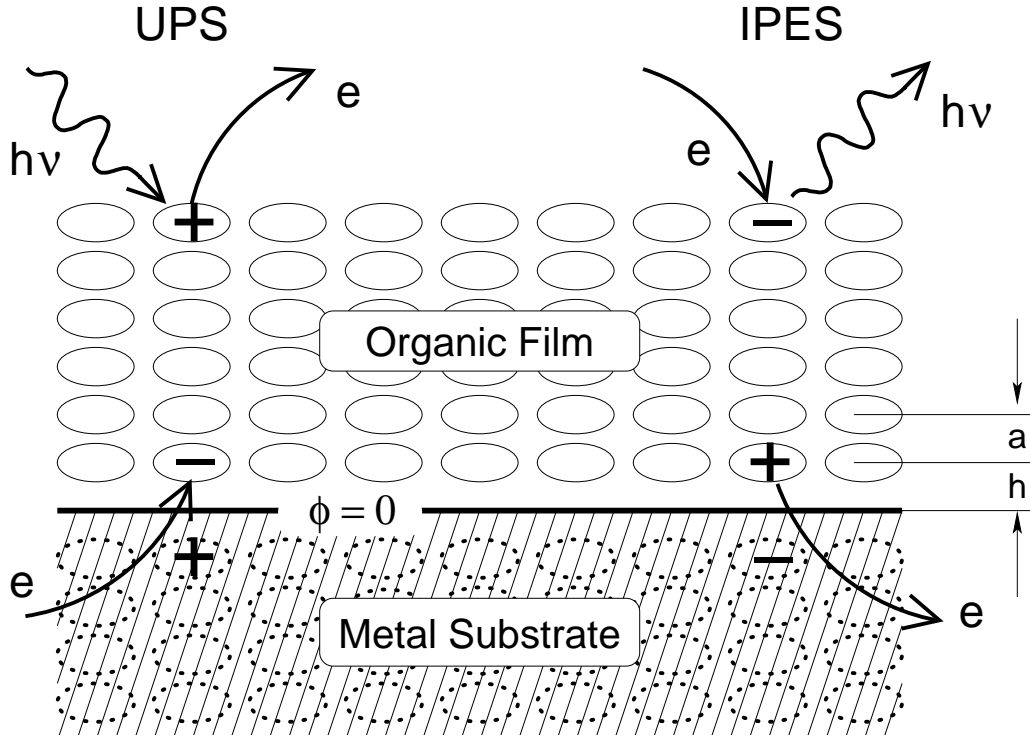


FIG. 2: Idealized model for electronic polarization in crystalline thin films on a metallic substrate at separation h . The N layers of the film appear as image charges. UPS and IPES generate a cation and anion at the surface, while charge injection generates ions in the interface layer.

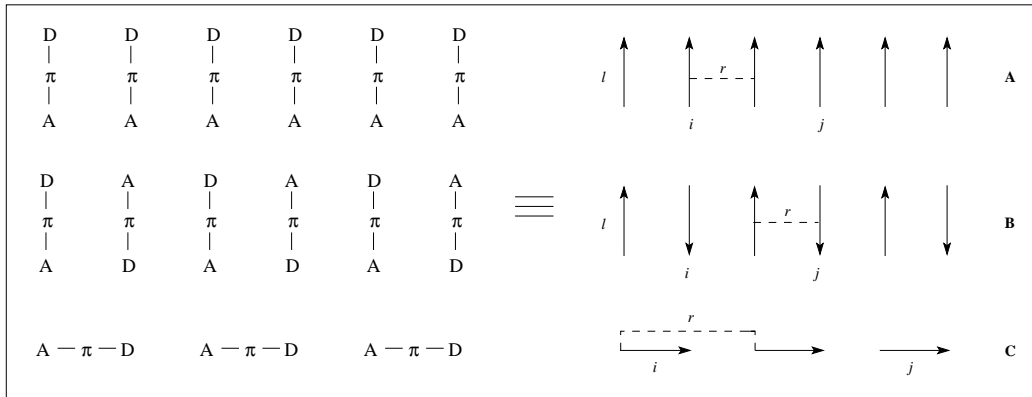


FIG. 3: Schematic view of the three one-dimensional clusters of polar and polarizable molecules considered in this work, the left panel shows the relative orientation of molecular dipole.

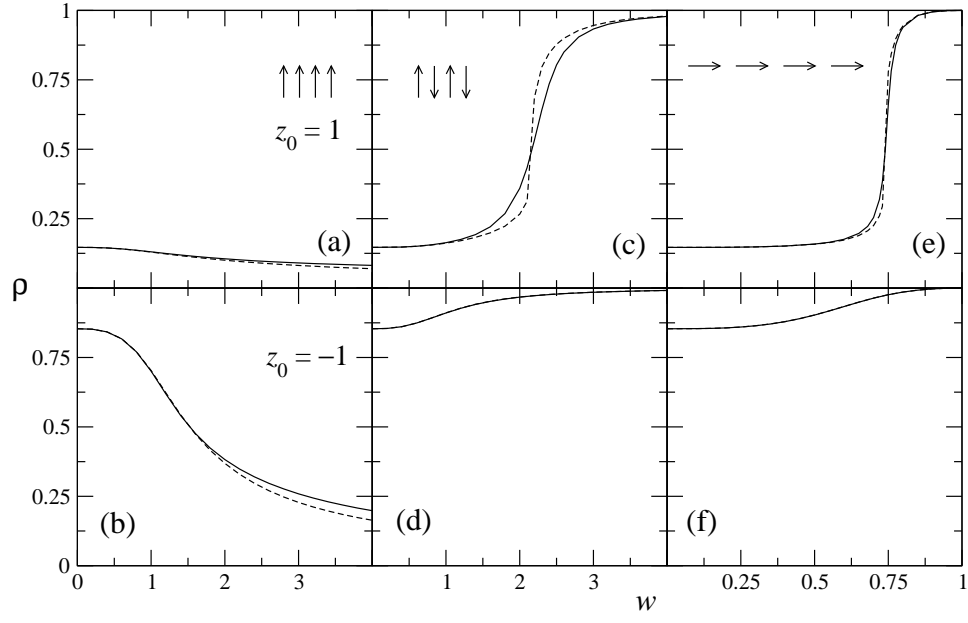


FIG. 4: Molecular ground state polarity, ρ , as a function of the strength of the interchromophore interaction, w , calculated for clusters of 16 molecules, with $v = 1$. Left, middle and right columns refer to geometries A, B and C, respectively; top and bottom rows correspond to $z_0 = 1$ and -1 , respectively. Continuous and dashed lines refer to exact and mean-field results, respectively. Finite size effects are negligible in all cases.

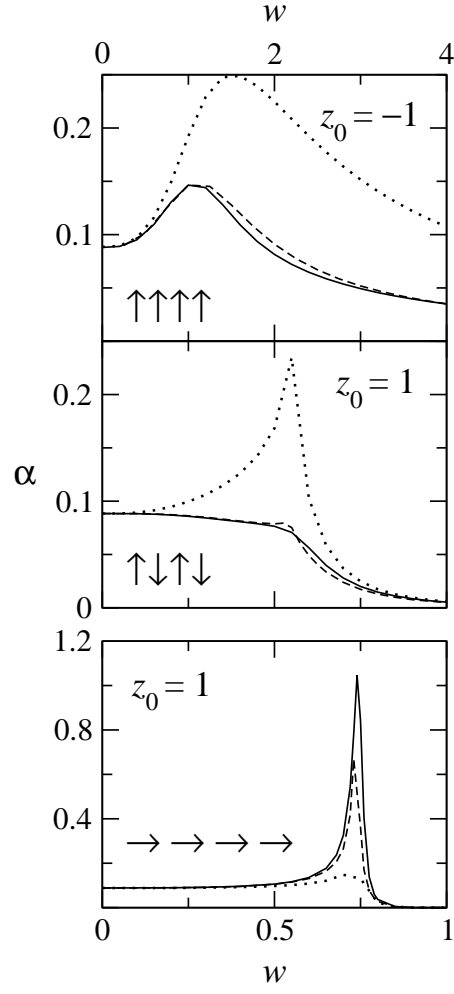


FIG. 5: Static polarizability calculated as a function of the strength of interchromophore interaction, w , for clusters of 16 molecules, with $v = 1$. Top panel: A geometry, $z_0 = -1$; middle panel: B geometry, $z_0 = 1$; bottom panels: C geometry, $z_0 = 1$. Continuous lines refer to the exact results, dashed lines to the mf-FF results, dotted lines to the mf-oriented gas results.

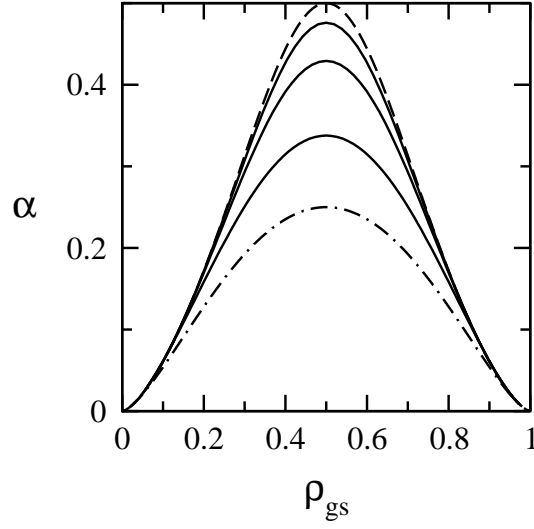


FIG. 6: Static polarizability as a function of the ground state ionicity ρ_{gs} , for $\epsilon_{sp} = 1$ and different ω values ($\sqrt{2}t$ units). Dashed line: potential energy contribution, corresponding to $\omega = 0$ limit (see text); dot-dashed line: bare electronic polarizability, corresponding to the $\omega \rightarrow \infty$ limit (see text); continuous lines report the exact polarizability calculated for $\omega = 0.05, 0.2, 1.0$, smoothly evolving from the $\omega = 0$ to the $\omega \rightarrow \infty$ limits; dotted line reports the polarizability calculated in the best harmonic approximation (see text). Dotted and dashed lines are exactly superimposed. For the calculation dipole moments have been expressed in μ_0 units.

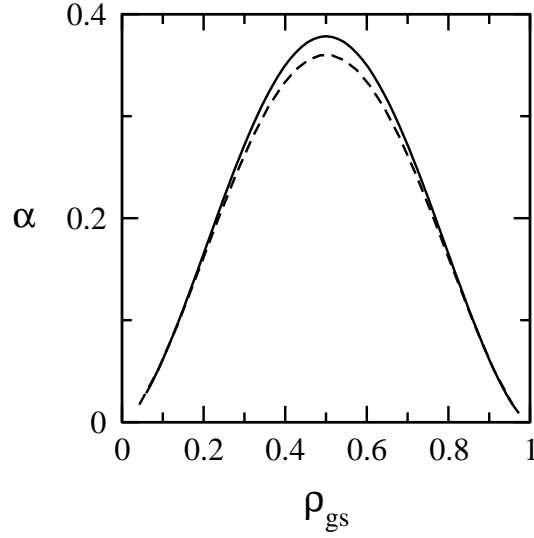
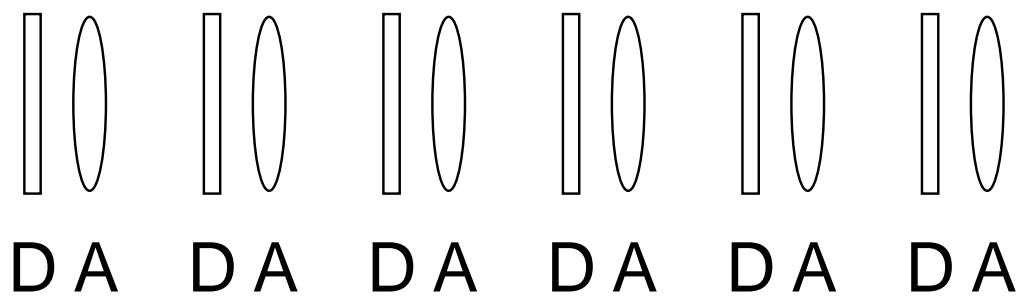
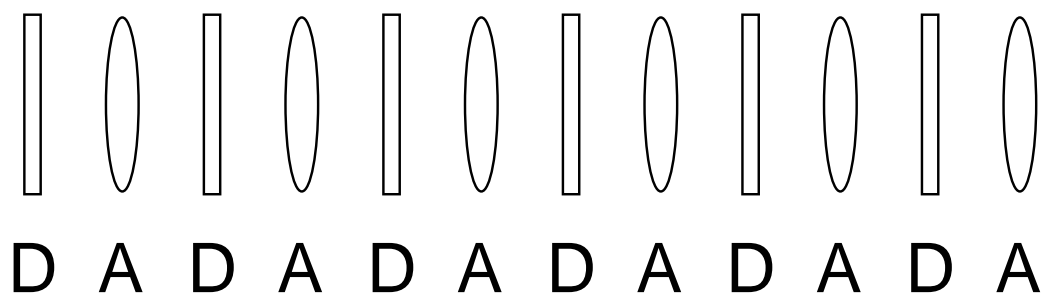


FIG. 7: Static polarizability as a function of the ground state ionicity ρ_{gs} , for $\epsilon_{sp} = 1$ and $\omega = 0.5$ ($\sqrt{2}t$ units). The continuous line shows the non-adiabatic result; the dashed line shows the BO result.

mixed regular stack



mixed dimerized stack

FIG. 8: A schematic view of mixed regular and dimerized stacks.

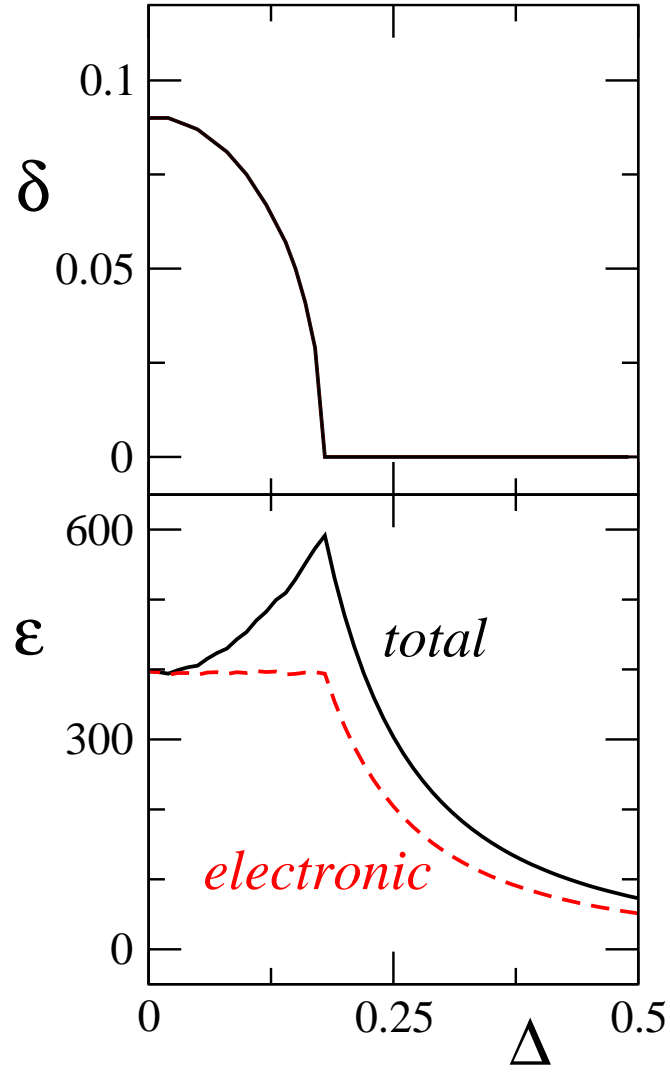


FIG. 9: The equilibrium dimerization amplitude δ and the electronic and total dielectric constants calculated for the hamiltonian in Eq. (8) with $U = 0$ and $\epsilon_d = 0.28$.